AIP | Journal of Applied Physics

Eu-activated fluorochlorozirconate glass-ceramic scintillators

J. A. Johnson, S. Schweizer, B. Henke, G. Chen, J. Woodford, P. J. Newman, and D. R. MacFarlane

Citation: Journal of Applied Physics **100**, 034701 (2006); doi: 10.1063/1.2225765
View online: http://dx.doi.org/10.1063/1.2225765
View Table of Contents: http://scitation.aip.org/content/aip/journal/jap/100/3?ver=pdfcov
Published by the AIP Publishing

Eu-activated fluorochlorozirconate glass-ceramic scintillators

J. A. Johnson[a)]
Energy Technology Division, Argonne National Laboratory, 9700 South Cass Avenue, Argonne, Illinois 60439

S. Schweizer
Energy Technology Division, Argonne National Laboratory, 9700 South Cass Avenue, Argonne, Illinois 60439 and Department of Physics, Faculty of Science, University of Paderborn, Warburger Str. 100, D-33095 Paderborn, Germany

B. Henke
Department of Physics, Faculty of Science, University of Paderborn, Warburger Str. 100, D-33095 Paderborn, Germany

G. Chen and J. Woodford
Energy Technology Division, Argonne National Laboratory, 9700 South Cass Avenue, Argonne, Illinois 60439

P. J. Newman and D. R. MacFarlane
Australian Centre for Electromaterials Science and School of Chemistry, Monash University, Clayton, Victoria 3800, Australia

(Received 4 March 2006; accepted 28 May 2006; published online 4 August 2006)

Rare-earth-doped fluorochlorozirconate (FCZ) glass-ceramic materials have been developed as scintillators and their properties investigated as a function of dopant level. The paper presents the relative scintillation efficiency in comparison to single-crystal cadmium tungstate, the scintillation intensity as a function of x-ray intensity and x-ray energy, and the spatial resolution (modulation transfer function). Images obtained with the FCZ glass-ceramic scintillator and with cadmium tungstate are also presented. Comparison shows that the image quality obtained using the glass ceramic is close to that from cadmium tungstate. Therefore, the glass-ceramic scintillator could be used as an alternative material for image formation resulting from scintillation. Other inorganic scintillators such as single crystals or polycrystalline films have limitations in resolution or size, but the transparent glass-ceramic can be scaled to any shape or size with excellent resolution. © *2006 American Institute of Physics*. [DOI: 10.1063/1.2225765]

I. INTRODUCTION

Eu-activated fluorochlorozirconate (FCZ) glass-ceramic materials have been developed as storage phosphors for medical applications, in particular, to replace the conventional screen/film system.[1–3] In this case x rays illuminate the glass-ceramic plate and create electron-hole pairs, which are stored until later released for recombination by a stimulating laser light. In the case of a scintillator, instead of storing the x-ray energy, it is directly converted into visible light. The materials described in this article are identical in nominal composition but have different heat treatment times and temperatures and can be used either as a storage phosphor or as a scintillator. In homeland security applications it is desirable to minimize the time for identification of any contraband material, so a scintillator is more appropriate. Some medical applications, such as mammography, are still based on imaging with storage phosphor where the image is read out some time after it is taken. However, techniques such as positron emission tomo-graphy or nuclear medicine are favorably disposed toward scintillation.

Traditional inorganic scintillators are CsI:Na, CsI:Tl, NaI:Tl, $CdWO_4$, and $Bi_4Ge_3O_{12}$ (BGO); see Refs. 4 and 5. They have light yields larger than 10 000 photons per MeV but decay times slower than 200 ns. On the other hand, the undoped halides BaF_2, CsF, CeF_3, and CsI, which have decay times in the range from 1 to 30 ns, have light yields of only a few thousand photons per MeV for the fast component.

Other materials include cerium-doped inorganics, Lu_2SiO_5:Ce, Gd_2SiO_5:Ce, $YAlO_3$:Ce, $LuAlO_3$:Ce, $Lu_2Si_2O_7$:Ce, and cerium-doped ^{6}Li glass.[4,5] Plastic scintillators,[6] anthracene and stilbene, are used almost exclusively as guard shields for low level counting due to their poor efficiency in detecting low energy x rays.

As no existing scintillator material has all the desired properties, there has been a search for different materials. The glass ceramics discussed in this article can be produced in any shape or size, including large-area detectors with very high resolution and adequate efficiency, and can be tailored to produce individual desirable properties for either medical or security applications. In addition, although at this point only tested with x rays, the material can be adapted to detect γ rays and neutrons with the substitution of appropriate glass formers and additional dopants.

[a)]Author to whom correspondence should be addressed; electronic mail: jaj2@anl.gov

II. EXPERIMENT

The Eu-doped FCZ glasses investigated are based on the well-known ZBLAN composition, which exhibits high stability against crystallization and has been used for fabricating infrared fibers.[7] The nominal composition of the FCZ glasses is 53 ZrF_4, 20 $BaCl_2$, 20 NaF $(4-x)$ LaF_3, 3 AlF_3, and x EuF_2, where $x=0.2,0.5,1,2$ (values are in mole %). The content of the substituted chlorine ions is close to 14% of the total number of anions. However, the actual chlorine content can be lower due to chlorine evaporation during the heating cycle.

The constituent chemicals were melted in a platinum crucible at 750 °C in an argon atmosphere and then poured into a brass mold, which was at a temperature below the glass transition temperature (T_g). The samples were annealed in a subsequent two-step heat treatment. In the first step they were exposed for 3 h to a temperature (200 °C) in the vicinity of T_g to produce a high density of crystal nuclei, and in the second step these nuclei were grown at 235 °C for 10 h. The material was then cooled to room temperature over 15 h. This overall treatment produces a large number of small crystallites. The glasses are transparent and have the potential to offer high spatial resolution. The dimensions of the glass ceramic plates are approximately 10 mm × 10 mm × 0.5 mm. These plates were polished with aluminum oxide-impregnated film, grit sizes 30 and 3 μm, to remove surface defects and thus improve image quality.

The x-ray excited luminescence (XL) spectra were detected using a 0.22 m double monochromator in combination with a cooled photomultiplier working in single-photon counting mode. The spectra were not corrected for spectral sensitivity of the experimental setup. The x-ray irradiation was carried out with a mobile x-ray tube using a tungsten anode at 60 kV and 15 mA.

An x-ray imaging system for testing the FCZ plates was built at the 2-BM beamline of the Advanced Photon Source (APS), Argonne National Laboratory. A schematic setup is shown in Ref. 8. A 5.5 mm (horizontal) × 3.8 mm (vertical) monochromatic x-ray beam is used as an imaging source. Although a synchrotron may seem to differ too greatly from normal medical x rays for this setup to be useful, synchrotron beams are being increasingly used for medical applications.[9] The x-ray beam passes through a phantom and projects its image on the FCZ plate. Many phantoms have been used to test the resolution of the glass-ceramic plates, in particular, the precision test pattern MA0647, which contains a series of parallel gold grids with spatial frequencies up to 20 line pairs/mm, and the mammography accreditation phantom 156 from Gammex RMI, which contains test objects that represent microcalcifications, fibrils, and tumor-like masses. In addition, a GaAs knife edge and a custom-made mask from the University of Wisconsin were used. The x-ray image on the sample is formed on a cooled charge-coupled device (CCD) camera through a 1.25X objective lens. In testing the glass-ceramic image plate for its scintillation properties, an image of the phantom is produced instantly and is formed on the CCD camera through an objective lens.

X-ray diffraction (XRD) experiments on the FCZ glass ceramics were performed at the 5-BM-C beamline of the APS. A monochromatic x-ray beam (wavelength = 0.334 861 Å) was selected by a Si (111) double crystal monochromator. The incident x-ray beam had a cross section of 1 mm (vertical) × 5 mm (horizontal). The samples (approx. 0.5 mm thick) were mounted at the center of a two-circle Huber powder diffractometer. Transmission geometry with 2-theta scanning was used, and a one-dimensional solid-state detector detected the diffracted x-ray beam. A standard Si polycrystalline sample from the National Institute of Standards and Technology was used to calibrate the diffraction angle (2-theta) and the x-ray wavelength.

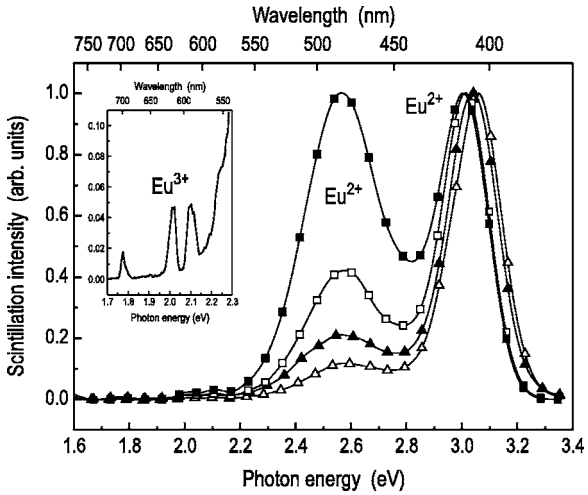

FIG. 1. X-ray excited luminescence spectra of double-annealed FCZ glass ceramics. The Eu doping level was 0.2% (open triangles), 0.5% (full triangles), 1% (open squares), and 2% (full squares). The inset shows the Eu^{3+} bands in the 2% sample before smoothing the spectrum.

III. RESULTS

Figure 1 shows the XL spectra of double-annealed FCZ glasses with a Eu doping level of 0.2%, 0.5%, 1%, and 2%. The XL for the 0.2% sample peaks at 407 nm with an additional weaker but broader peak at 485 nm; both peaks are observed only in glass ceramics containing hexagonal $BaCl_2$ nanoparticles; this has been shown previously by photoluminescence measurements.[2] The peak at 407 nm is attributed to the $5d$-$4f$ transition of Eu^{2+} present in the hexagonal $BaCl_2$ nanoparticles, whereas the origin of the 485 nm peak is unknown. Interestingly, the peak at 485 nm grows from a relatively small bump at 0.2% Eu^{2+} doping level to comparable intensity with the peak at 412 nm when the Eu^{2+} doping level reaches 2%. The peak height at 485 nm scales approximately linearly with europium doping. It should also be noted that in the 1% and 2% Eu^{2+}-doped samples, there is a shift in the peak from 407 to 412 nm. In addition to the Eu^{2+} emissions, typical transitions from Eu^{3+} were observed in the fluorozirconate glass matrix.[10] The inset shows the Eu^{3+} bands in the 2% sample before smoothing the spectrum.

Figure 2 shows the relative efficiency for the different europium doping levels. The efficiencies were calculated by measuring the light intensity in a predetermined rectangle of the image in comparison to cadmium tungstate (CWO), exposed under the same conditions. All samples were of the

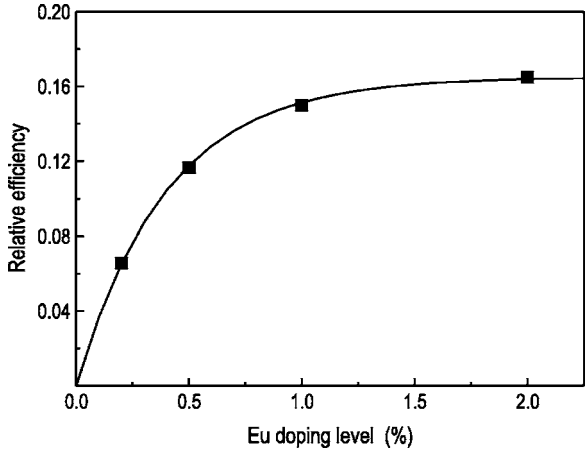

FIG. 2. Relative scintillation efficiency compared to cadmium tungstate of double-annealed FCZ glass ceramics for various Eu-doping levels. The line is a guide to the eye.

same thickness, ≈500 μm. A monochromatic beam at 16 keV was used with an acquisition time of 15 s. The figure shows a maximum at a doping level of 2% Eu compared to CWO-normalized relative values.

Figure 3 shows a typical XRD pattern from which the structure and approximate size of the crystallites can be determined. The sharp peaks superimposed on the glassy background were identified as arising from hexagonal $BaCl_2$.[11] The software package GSAS[12] was employed to perform a Rietveld analysis of the patterns. The average crystallite size was found to be 14±2 nm at all doping levels. Some peak broadening due to lattice distortion is likely to be present as well, but the magnitude of the broadening was determined to be within the error of the particle size, so useful information could not be extracted. The XRD pattern of hexagonal $BaCl_2$ (bottom bar graph, PDF 45-1313) is also shown.

Figure 4 gives the scintillation intensity as a function of x-ray intensity. These measurements were performed at 16 keV, and the x-ray intensity was reduced by a series of aluminum filters. Acquisition times varied from 3 s to 30 min, depending on the x-ray intensity. At low x-ray intensity longer acquisition times were needed to overcome a problem with signal-to-noise ratio. The scintillation efficiency scales linearly with x-ray intensity over the range measured. The deviation of the 0.2% sample from the slope of the CWO and 2% sample is likely due to the poor signal-to-noise ratio at low intensity.

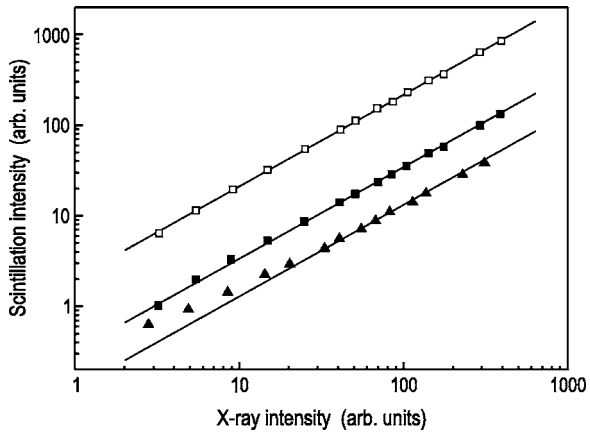

FIG. 4. Scintillation intensity vs x-ray dose of Eu-doped, double-annealed FCZ glass ceramics (full symbols). The Eu doping level was 0.2% (triangles) and 2% (squares). The scintillation efficiency of cadmium tungstate is shown for comparison (open squares). The lines for the CWO and 2% Eu data are a linear fit; the 0.2% data are believed to be inaccurate at low x-ray intensity, and so the line is made parallel to the other two lines.

Figure 5 shows the energy-dependent scintillation intensity of all the Eu^{2+}-doped scintillators studied in this paper (0.2% to 2% doping level). The scintillation intensity increases exponentially with x-ray energy. The only anomaly in this increase is that the Zr edge becomes increasingly sharp with doping level. Future experiments will test the response of the material at a higher energy beam line to determine where the intensity saturates.

Figure 6 shows the modulation transfer function (MTF) versus spatial frequency for CWO and the 2% Eu-doped FCZ glass ceramic. The graph gives a measure of the image quality from the relative contrast of an imaging system as a function of spatial frequency. The resolution is defined as the

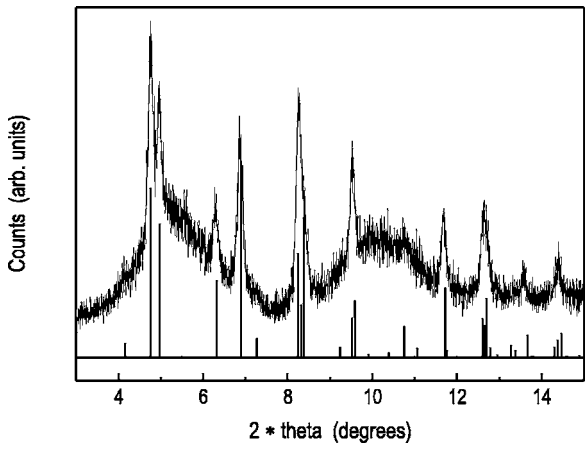

FIG. 3. The XRD pattern of a double-annealed 2%-Eu-doped ZBLAN glass ceramic. Pattern indicates an amorphous phase and a hexagonal $BaCl_2$ phase with an average crystallite size of 14±2 nm. The XRD pattern of hexagonal $BaCl_2$ (bottom bar graph, PDF 45-1313) is also shown.

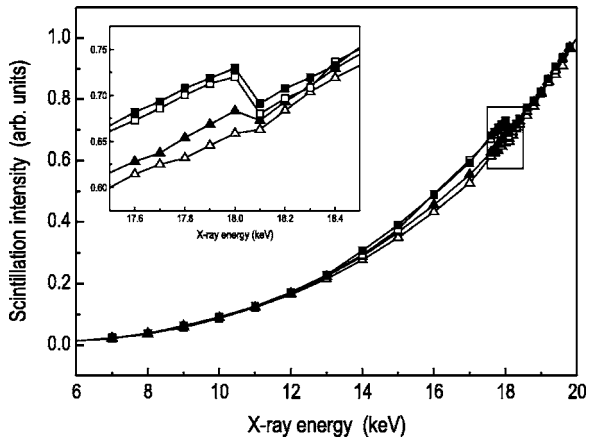

FIG. 5. Scintillation intensity vs x-ray energy of Eu-doped, double-annealed FCZ glass ceramics. The Eu-doping level was 0.2% (open triangles), 0.5% (full triangles), 1% (open squares), and 2% (full squares). The lines are a guide to the eye, whereas the symbols represent the experimental data points. The inset shows the Zr edge at 18 keV.

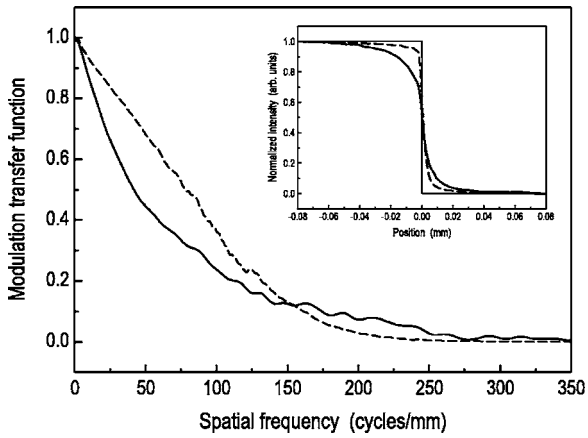

FIG. 6. The MTF of a 2% Eu-doped, double-annealed FCZ glass-ceramic scintillator (solid curve). The MTF of CWO (dashed curve) is shown for comparison. The inset shows the scintillation intensity profile for the FCZ plate (solid curve) and the CWO single crystal (dashed curve). The ideal profile (thin solid curve) is shown for comparison.

value of the spatial frequency corresponding to a certain MTF value. Here, the value of resolution is taken at an MTF of 0.2. The resolution of the scintillator system is $\approx$110 lp/mm (at MTF=0.2). In other words, this system is able to resolve features as small as 4–5 μm. The resolution of CWO is $\approx$130 lp/mm, which implies it can detect features of just less than 4 μm.

IV. DISCUSSION

Ideally, to interpret the XL spectra the results should be compared to bulk hexagonal $BaCl_2$ but this comparison is difficult since this material cannot easily be made.[11] In fluorozirconate glass ceramics containing small hexagonal $BaBr_2$ crystallites[13,14] or small hexagonal $BaCl_2$ crystallites,[2] a band near 485 nm was reported. Edgar *et al.* speculated that the band arises from an Eu^{2+} ion associated with an impurity in the hexagonal phase, which disappeared after heat treatment, and the simultaneous transformation to the orthorhombic phase. The initial hexagonal phase is expected to contain a significant fraction of impurities from the glass. In the glass-ceramic samples, thermal treatments are identical and only differ in europium concentration; the crystallites are always in the hexagonal phase. The fact that the band scales linearly with europium doping is a significant and important result. As yet there is no explanation for this finding and it can only be surmised that Edgar's speculation is correct. In addition, there is a shift in the 407 nm peak to 412 nm when the doping level is increased from 0.2% to 2%. This shift could be due to overlapping bands, self-absorption by europium, or a perturbed crystal field. Further luminescence experiments will be performed to resolve this issue and will be the subject of a separate paper.

The efficiency of the glass-ceramic plate is an extremely important parameter for medical applications. A patient must be exposed to the minimum possible dose; radiation dose is less important in homeland security applications, where image quality and speed are paramount. Figure 2 shows that efficiency increases with respect to europium doping level but levels off rather quickly. This result implies that little would be gained in efficiency by increasing the europium-doping level beyond 2%. There is also a limit to how much europium can be incorporated into the material as this element creates nucleation sites, which lead to crystallization. The maximum efficiency of 16% compared to CWO in the samples examined here is the lower limit. The material and the readout system can still be improved. The present optical system is optimized for CWO. A photomultiplier should ultimately be used and attached directly to the image plate. In addition, improved synthesis methods could help retain more chlorine, as some is undoubtedly lost in the melting process.

X-ray diffraction provides structural information, specifically crystalline phase identity, average crystallite size, and if the signal-to-noise is high, the average stress or strain on crystallites. The XRD pattern shown in Fig. 3 is of a 2%-Eu-doped glass-ceramic plate, which was double-annealed for 20 h and had the highest scintillation efficiency of all the glass-ceramic samples. The two broad humps centered around 5.5° and 10.5° are the glassy background arising from the amorphous glass matrix. The sharp peaks superimposed on the broad humps are the diffraction peaks of the crystalline phase, hexagonal $BaCl_2$ in this case. The average crystallite size, $\approx$14 nm, is much smaller than the wavelength of visible light. Therefore, light scattering due to particle size is negligible, and the glass ceramic is fully transparent. This behavior is important to resolution; resolution is soon lost once the particle size approaches the wavelength of light. Clarity of the image is crucial in both medicine and homeland security applications.

The scintillation efficiency is linear over almost three orders of magnitude. At low x-ray intensity the signal-to-

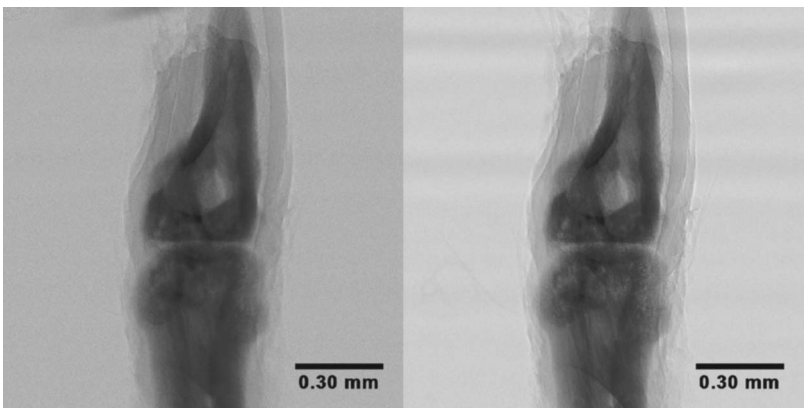

FIG. 7. Scintillation image of a mouse joint, recorded with a double-annealed 2% Eu^{2+}-doped FCZ plate (left) and with a CWO single crystal (right).

noise ratio is higher for equal time intervals; therefore, scan length was increased to compensate for this. For homeland security applications, where dose does not matter, maximum x-ray intensity will be investigated (eventually the efficiency will saturate) so that efficiency can be maximized and the time to obtain an image shortened without compromising resolution.

Figure 5 shows that the scintillation intensities of the glass ceramics with different doping levels follow the same curve. It increases quasi exponentially with x-ray energy and is proportional to the inverse mass absorption coefficient;[15] that is, the more photoelectric absorption, the less scintillation. The zirconium K edge is sharp in the 1% and 2% sample, less sharp in the 0.5% sample, and hardly noticeable in the 0.2% sample. The fluorozirconate glass matrix obviously has an influence on the scintillation intensity of the glass ceramic. However, the inset in Fig. 5 shows that the intensity drop at 18 keV is not as absolute as one would expect from the (inverse) mass attenuation coefficient but varies from sample to sample; this variation is probably caused by the different lifetimes of the ionized Zr. It seems that the lifetime of the ionized Zr is influenced by the size, structure, and composition of the embedded nanoparticles. Note that the chemical composition does not change during thermal processing.

The MTF curves shown in Fig. 6 indicate that in terms of resolution the glass-ceramic plate is almost state of the art but would only cost a fraction of the single-crystal CWO. This statement is supported by the image of a mouse leg in Fig. 7, where the detailed structure of the bones is clearly resolved in both images-the Eu^{2+}-doped scintillator is on the left, and CWO is on the right.

V. CONCLUSIONS

A scintillator image plate has been designed and tested. The relative efficiency of the plate was compared to CWO, a typical tomography scintillator, and was found to be 16% at the 2% Eu-doping level. The scintillation mechanism was found to derive from Eu^{2+} incorporated into hexagonal phase $BaCl_2$ nanocrystallites in the glass. Over the range measured, scintillation intensity was linear as a function of x-ray intensity. Future experiments will test the linearity and response of the material at higher energies. The energy-dependent scintillation intensity increased exponentially with x-ray energy, except at the zirconium edge. Further experiments will determine the saturation level. Finally, the plate is shown to have very high resolution, 110 lp/mm at a MTF of 0.2. Further development of the plate will focus on increasing the efficiency and synthesizing a material that will respond to other forms of radiation such as γ rays and neutrons.

ACKNOWLEDGMENTS

The authors would like to thank F. De Carlo of the Argonne National Laboratory for his help with the experiment, and A. Edgar for useful discussions. Use of the Advanced Photon Source was supported by the U.S. Department of Energy, Office of Science, Office of Basic Energy Sciences, under Contract No. W-31-109-Eng-38. This work was supported by the National Institutes of Health under Grant No. R21 EB02928.

[1] S. Schweizer, L. W. Hobbs, M. Secu, J.-M. Spaeth, A. Edgar, and G. V. M. Williams, Appl. Phys. Lett. **83**, 449 (2003).
[2] S. Schweizer, L. W. Hobbs, M. Secu, J.-M. Spaeth, A. Edgar, G. V. M. Williams, and J. Hamlin, J. Appl. Phys. **97**, 083522 (2005).
[3] G. Chen, J. A. Johnson, R. Weber, S. Schweizer, D. MacFarlane, J. Woodford, and F. De Carlo, Proc. SPIE **5745**, 1351 (2005).
[4] C. W. E. van Eijk, Nucl. Instrum. Methods Phys. Res. A **460**, 1 (2001).
[5] C. W. E. van Eijk, Phys. Med. Biol. **47**, R85 (2002).
[6] M. G. Schorr and F. L. Torney, Phys. Rev. **80**, 474 (1950).
[7] I. D. Aggarwal and G. Lu, *Fluoride Glass Fiber Optics* (Academic, Boston, 1991), Chap. 1.
[8] G. Chen, J. Johnson, R. Weber, R. Nishikawa, S. Schweizer, P. Newman, and D. MacFarlane, J. Non-Cryst. Solids **352**, 610 (2006).
[9] M. J. Yaffe and J. A. Rowlands, Phys. Med. Biol. **42**, 1 (1997).
[10] L. Samek, J. Wasylak, and K. Marczuch, J. Non-Cryst. Solids **140**, 243 (1992).
[11] G. Liu and H. A. Eick, J. Less-Common Met. **149**, 47 (1989).
[12] A. C. Larson and R. B. Von Dreele, General Structure Analysis System (GSAS), Los Alamos National Laboratory Report No. LAUR 86-748 (2004).
[13] A. Edgar, M. Secu, G. V. M. Williams, S. Schweizer, and J.-M. Spaeth, J. Phys.: Condens. Matter **13**, 6259 (2001).
[14] M. Secu, S. Schweizer, J.-M. Spaeth, A. Edgar, G. V. M. Williams, and U. Rieser, J. Phys.: Condens. Matter **15**, 1097 (2003).
[15] S. Schweizer, B. Henke, S. Köneke, J. A. Johnson, G. Chen, and J. B. Woodford, Proc. SPIE **6142**, 61422Y (2006).